Investigation of symmetric splitting and jetting of bubbles in phosphoric acid

Max Koch[1], Juan M. Rosselló[2], Christiane Lechner[3], Robert Mettin[1*]
[1]*Drittes Physikalisches Institut, Georg-August-Universität Göttingen, Friedrich-Hund-Platz 1, 37077 Göttingen, Germany*
[2]*Instituto Balseiro-CONICET, Centro Atómico Bariloche, Río Negro R8402AGP, Argentina*
[3]*Institute of Fluid Mechanics and Heat Transfer, TU Wien, Getreidemarkt 9, Vienna 1060, Austria*
[*]*Email: Robert.Mettin@phys.uni-goettingen.de*

Introduction

Bubbles in viscous liquids have attracted some interest recently due to the extremely bright sonoluminescence flashes of collapsing noble gas bubbles in acids [1, 2, 3, 4, 5] that are partly visible with the unaided eye in daylight environment. The deeper reasons for the spectacular brightness are not yet fully clear. The low vapor pressures of sulfuric and phosphoric acid seem to be responsible for part of the boosting [6]. Also, the flashing bubbles in these acids appear to be rather large and spherically stable as compared to bubbles in water [7, 5]. Thus a closer consideration of bubble dynamics in acids is motivated to highlight differences to other liquids.

Several studies have investigated trapped bubbles in acids experimentally and numerically [1, 3, 4, 6, 8], where usually spherical bubble shape is observed or supposed. Here we report on two approaches to study non-spherical bubble dynamics in phosphoric acid: Firstly, we conduct experiments with a trapped and slowly moving argon bubble (the translations being similar to that in moving-SBSL states [9, 10]). We find a peculiar repetitive symmetric bubble splitting during the collapse phase (with re-merging during expansion) that appears long-term stable without destroying the bubble. Secondly, we perform numerical simulations of a laser pulse induced jetting bubble close to a rigid boundary. Several differences to a similar jetting bubble collapse in water occur.

Experiments

Experimental setup. The acoustic chamber used in the experiments was made from a cubical optical glass flask (*Hellma)* with 5 cm of inner length and a wall thickness of 2.5 mm. The cuvette has two opposite ports at the corners of the top and bottom faces as shown in Figure 1. The bottom port was coupled to a transparent teflon tube and was used as an auxiliary port to fill the flask with the liquid stored in a second reservoir, which was used to degas and dissolve some noble gas in the liquid. This fluid handling system allowed us to transfer a phosphoric acid aqueous solution 85% w/w (PA85) to the test cell without exposing it to air.

The driving system was built with three disc shaped piezo ceramics transducers (PZT) with 2.5 cm of diameter attached to the wall faces using epoxy resin. The ultrasound pressure signal was measured with a smaller PZT, which measures a voltage proportional to the acceleration of the flask wall acting as a microphone (MIC) (see Fig. 1).

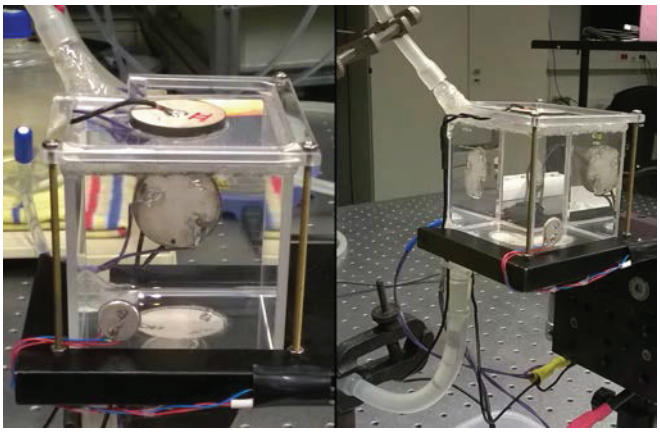

Figure 1: Two views of the cubical acoustic chamber used in the cavitation experiments. The service ports (hoses) were employed to fill the vessel with the working liquid (PA85 with some mbars of argon dissolved) without contamination. The laser induced bubbles were driven with a fundamental frequency $f_0 = 25.1$ kHz plus its third harmonic ($3f_0$) by the three larger piezo ceramic discs. A smaller piezo ceramic is used as a pickup receiver. The resonator was hermetically sealed and acid resistant.

The sinusoidal driving signal was generated using a *Yokogama FG120* function generator with two phase locked independent channels. The low frequency component of the bi-harmonic signal (V_{PZT}^{LF}) was amplified with a *t.amp TA550* 500 W audio amplifier and boosted with a tunable RLC circuit which permits us to attain typical maximum output values of 400 V_{rms}. The high frequency signal was amplified (*NS-HS4101* HF amplifier, 400 W) and connected via a second RLC circuit. The two opposite PZT drivers were used for the harmonic frequency component (Nf_0), while the remaining one was used for the low-frequency signal (f_0). The main resonance frequency of the entire system was experimentally determined to $f_0 = 25.1$ kHz. That frequency matches oscillation mode (1,0,1) with a pressure antinode in the geometrical center of the flask. The room temperature was close to 295 K in all the measurements.

Individual bubbles were generated focusing a high power laser pulse from a Nd-YAG laser (*Spectra-Physics Quanta-Ray PIV)* near the center of the flask. Bubbles were instantly trapped within the acoustic field. The bubble dynamics was

characterized by analyzing a series of high speed videos (300 kfps or 420 kfps) of the bubble oscillations, using a *Photron Fastcam SA5* in combination with a long distance microscope *Infinity K2* as shown in Fig. 2. In all the measurements we used backlighting technique and the highest shutter speed (368 ns) to produce resolved images with sharp edges.

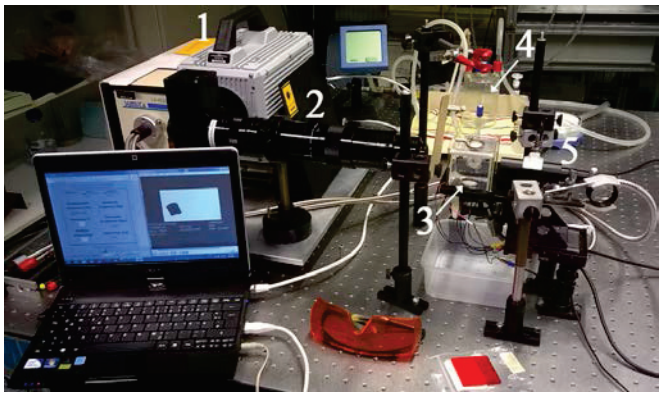

Figure 2: Detail of the experimental setup. The main components were: 1) High speed camera. 2) Long distance microscope. 3) Cubical resonator. 4) Gassing/degassing system. 5) High intensity lamp.

Bubble dynamics. An example of a typical trapped bubble behavior in PA85 is shown in Fig. 3. The bubble undergoes strong expansion-collapse oscillations of repetitive manner. At the same time its center position moves slowly with velocities of the order of 0.1 m/s in apparently erratic loops near the pressure antinode (direction of motion in Fig. 3 is from bottom right to upper left). The bubble shape appears close to a sphere when expanded, as an oblate ellipsoid perpendicular to the traveling direction during the shrinking phase, and as a prolate ellipsoid stretched along the traveling direction during re-expansion. Closer inspection exhibits always slight deformation of the bubble from spherical shape and a flip from prolate to oblate ellipsoid near the maximum expansion, indicating a sustained n = 2 surface mode oscillation. Probably the volume oscillation with driving frequency f_0 is in resonance to the n = 2 mode, but a detailed investigation needs an estimation of the bubble's equilibrium radius R_0 which could be done via a dynamics fit with a spherical bubble model [7]. The peculiar splitting in the collapse (Fig. 4) appears to be triggered by an annular inward jet, i.e. the higher curvature sides of the oblate bubble turn inwards and form a sharp and deep constriction towards the symmetry axis. Figure 5 gives a picture of the supposed full dynamics. From the recordings it is not clear if the bubble is finally really split into separate daughter bubbles, or if a gas bridge is sustained (possibly both might occur, and also a gas bridge might rupture later during the rebound). In any case, the re-expanding bubble parts merge and form a nearly spherical bubble again afterwards. For single collapse events of ellipsoidal bubbles in water, similar jetting geometry appears [11]. However, it is supposed that the high viscosity of the acid plays a crucial role for the extreme reproducibility of the collapse splitting, which is to our knowledge not seen in water.

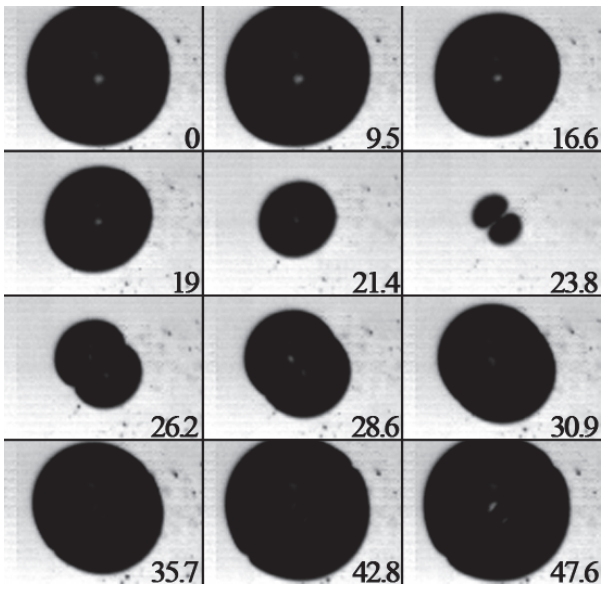

Figure 3: Image sequence of a splitting bubble collapse (frame width ≈ 840 µm). The working liquid was PA85 with argon dissolved. The bi-frequency driving signal has f_0 = 25.1 kHz, N = 3, P_{Ac}^{LF} = 440 V_{rms} and P_{Ac}^{HF} = 80 V_{rms}. The numbers in the corner of each frame indicate the time in µs. The maximum radius reached by the bubble was ≈ 320 µm.

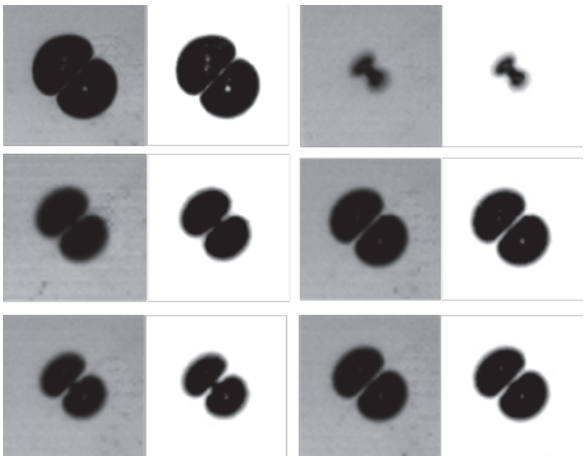

Figure 4: Selection of bubble snapshots taken at the instant where the splitting occurs. The contrast of the pictures was increased in order to highlight the bubble fracture. The width of the frames is ≈ 245µm.

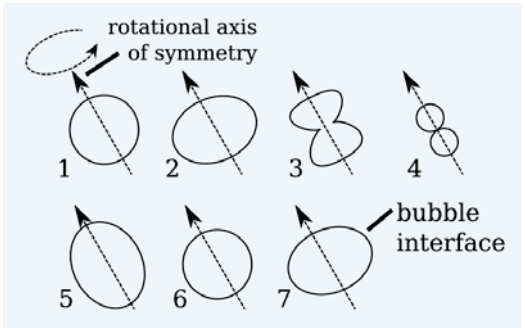

Figure 5: Sketch of the temporal sequence of the repetitive symmetric splitting of the bubble under n = 2 instability. The cycle starts again after "5", i.e. "6" = "1", "7" = "2".

Simulations

Code. Simulations of a collapsing bubble in front of a solid wall both in water and PA85 were performed with a Finite Volume solver based on the open source CFD package OpenFOAM [12], see [13, 14]. The solver was developed during the last three years to an extent where laser induced cavitation bubbles can be simulated very accurately including nonlinear compressibility effects, such as shock waves, and topology changes of the bubble. The code was extensively tested for a bubble expansion, collapse and rebound in front of a rigid wall. Therefore, in this paper we present a comparison of the phenomena of water and PA85 for such a case (Implementation of ultrasonic driving and ellipsoidal initial conditions to attack as well the observed repeated collapse splitting events is under development.) As advancement of the code in [13, 14], the results shown in this paper include yet unpublished modifications concerning local correction of the mass error in the computational cells on the bubble interface. The details of these findings will be described in detail in the future and are omitted here.

Results. Figure 6 shows the numerical simulation of a laser induced cavitation bubble for water (left) and PA85 (right) for different stages of bubble evolution. The bubble is filled with non-condensable air and does not contain vapour. Since the liquid density and liquid viscosity (as well as the surface tension and sound speed) differ in both liquids, the collapse times deviate, and thus similar bubble evolution stages appear at different absolute times. The equilibrium radius of the bubble was set to 80 µm and the starting radius was 50 µm, thus realizing an isentropically compressed bubble pressure at t = 0 s. A non-zero initial velocity field directed outwards was added such that a stronger expansion up to ≈ 450 µm occurs. For water, the interface velocity was set to 227 m/s. In PA85, in order to reach closely the same maximum bubble radius as in water, the velocity had to be less (162.06 m/s) due to the higher liquid density. Note that horizontal spatial scales (left and right hand side) in Fig. 6 are matched, but vertically (from top to bottom) the scales are adjusted in order to better visualize the dynamics. The general bubble collapse dynamics near a solid boundary is discussed, for instance, in [15]. Figure 6 shows in the first line the pressure field at maximum bubble expansion, the second line the pressure at the first bubble collapse to a thin torus (with hardly discernible, strongly compressed gas phase and out-running shock wave). Third and fourth line show the velocity field of liquid jet penetration and the end state after the second collapse and rebound. It can be seen that the bubble in PA85 travels further towards the rigid wall (bottom) and collapses more towards a “point” (i.e. with a better defined collapse ring). The pressure peak of the shock wave in PA85 also reaches a little higher value than in water. The rebound with the central liquid jet flow reveals nearly identical jet velocities, while the equivalent bubble radius at maximum rebound is smaller for PA85. The bubble shape for the stage of liquid jet penetration seems more disturbed for PA85, but this characterization interchanges later when it comes to the velocity field of the end-state: in water the remnant bubbles induce complex vortices, while in PA85 the flow field looks more laminar and lacks smaller scale features – as expected due to the smaller Reynolds number. Further consequence of the higher viscosity seems to be a thicker liquid layer between bubble and solid in the case of PA85.

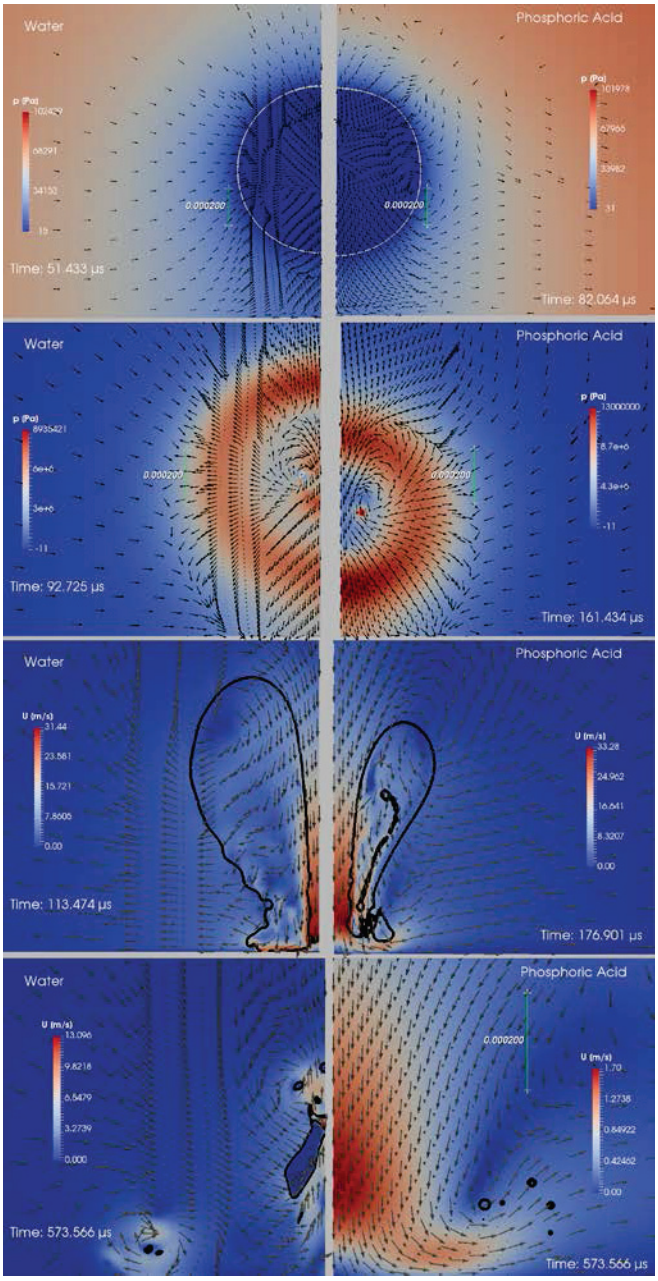

Figure 6: Selected frames from the numerical calculations of collapsing laser induced bubbles above a solid boundary (at the bottom of the images; axisymmetric calculations, symmetry axis in the centre between columns). Normalized distance of initial bubble centre of mass to the boundary $d/R_{max} = \gamma \approx 1.7$. Left column: bubble in water; right column: bubble in PA85. Times given relative to bubble initialization; frames selected for similar states of collapse dynamics (see text).

Figure 7 shows the time development of the equivalent bubble radii of the numerical solutions for both liquids. A significant prolongation of the collapse time in PA85 (mainly due to the higher density) is clearly visible here, also the smaller maximum rebound radii, already discussed in the context of Fig. 6.

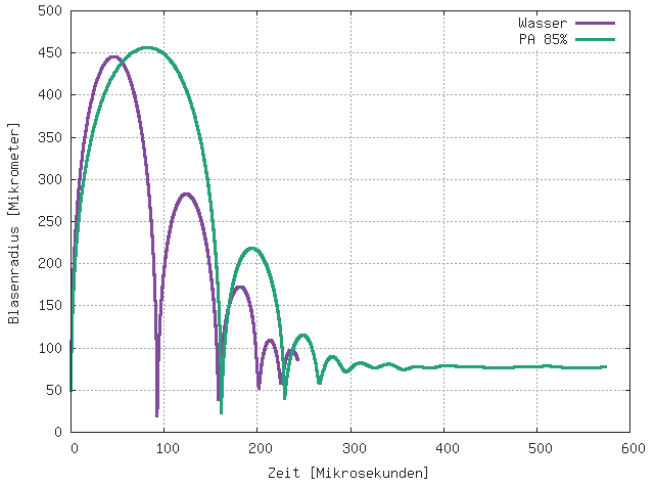

Figure 7: Radius vs. time traces of water and PA85 bubbles collapsing close to a solid boundary (as in Fig. 6). Time given relative to bubble initialization, and radius corresponds to an equivalent spherical bubble of the same gas volume.

Discussion and outlook

We have reported two cases of non-spherical bubble dynamics in phosphoric acid: (i) an experiment where an acoustically trapped bubble undergoes repeated, periodic symmetric splitting during its collapse phase, and (ii) numerical calculation of the collapse of a laser induced bubble close to a rigid boundary in comparison to the collapse in water. The case (i) appears to be triggered by a resonance of the n = 2 shape mode with the acoustic driving frequency, and the high viscosity of the acid seems to play a crucial role in stabilizing the bubble oscillation in the sense of a non-destructive, periodic rebound to (nearly) spherical shape. The case (ii) highlights similarities and changes that occur in the jetting bubble dynamics for raising the liquid viscosity from that of water. While the general jetting scenario and the jet flow velocity remain similar, the reduced Reynolds number suppresses smaller scale vortex dynamics that follow the collapse in water [16] (a rough estimation for the jet flow of about v=30m/s and a diameter of D=100µm results in $Re = \rho v D/\mu \approx 3000$ for water and $Re \approx 250$ for PA85). Also, the rebounds are significantly smaller in acid than in water. This is possibly due to viscous losses, but also higher radiated energy in the shock wave might contribute since the first (ring) collapse appears more focused in the acid. Furthermore, the higher density of the acid leads to a prolongation of the collapse time.

Future numerical work will elaborate the detailed reasons for the observed differences in the jetting collapse scenario (ii). It will also be tried to include acoustic driving and non-spherical initial conditions to model the experimental case (i) and explore the small scale dynamics of this peculiar bubble behavior.

Acknowledgement: J.M.R. was supported with a postdoctoral scholarship granted by the National Research Council of Argentina (CONICET). The authors thank all members of the cavitation group at Drittes Physikalisches Institut for help and valuable discussions. Particular thanks go to Werner Lauterborn for very helpful comments and discussions in the tea break.

References

[1] A. Troia, D. Madonna Ripa, R. Spagnolo, Ultrason. Sonochem. 13, 278 (2006).

[2] K. S. Suslick, N. C. Eddingsaas, D. J. Flannigan, S. D. Hopkins, and H. Xu, Ultrason. Sonochem. 18, 842 (2011).

[3] J. M. Rosselló, D. Dellavale, F. J. Bonetto, Phys. Rev. E 88, 033026 (2013).

[4] J. M. Rosselló, D. Dellavale, F. J. Bonetto, Ultrason. Sonochem. 31, 610 (2016).

[5] C. Cairós, R. Mettin, Phys. Rev. Lett. 118, 064301 (2017).

[6] S. D. Hopkins, S. J. Putterman, B. A. Kappus, K. S. Suslick, C. G. Camara, Phys. Rev. Lett. 95, 254301 (2005).

[7] A. Thiemann, F. Holsteyns, C. Cairós, R. Mettin, Ultrason. Sonochem. 34, 663 (2017).

[8] A. Moshaii, M. Faraji, and S. Tajik-Nezhad, Ultrason. Sonochem. 18, 1148 (2011).

[9] Y. T. Didenko,W. B. McNamara, and K. S. Suslick, Nature (London) 407, 877 (2000).

[10] R. Toegel, S. Luther, D. Lohse, Phys. Rev. Lett. 96, 114301 (2006).

[11] K. Tsiglifis, N. A. Pelekasis, Ultrason. Sonochem. 14, 456 (2007).

[12] OpenFOAM-extend project community OpenFOAM-extend project, download at http://sourceforge.net/projects/openfoam-extend/files/foam-extend-3.0/ (June2014), http://www.extend-project.de/.

[13] M. Koch, Ch. Lechner, F. Reuter, K. Köhler, R. Mettin, W. Lauterborn, Computers and Fluids 126, 71 (2016).

[14] M. Koch. Ch. Lechner, F. Reuter, R. Mettin, W. Lauterborn, in: M. Vorländer, J. Fels (Eds.): Fortschritte der Akustik - DAGA 2016 Aachen (DEGA, Berlin, 2016), pp. 93-96.

[15] O. Lindau, W. Lauterborn, J. Fluid Mech. 479, 327 (2003).

[16] F. Reuter, C. Cairós, R. Mettin, Ultrason. Sonochem. 33, 170 (2016).